Effect of Induced Lateral Displacement on Vertically Loaded Large Piled-Raft Response in Sandy Soil

Banchiva K. Marak[1]* and Baleshwar Singh[1]

[1]Civil Engineering Department, Indian Institute of Technology Guwahati, Assam, India, 781039

*Corresponding author's email: banchivakmarak94@gmail.com

Abstract. The lateral displacement can also be induced in the piled-raft foundations (PRFs) for onshore structures in addition to vertical load on account of the excavations carried out very close to the existing PRFs. In the present study, three-dimensional numerical analyses are performed on vertically loaded large PRFs in dense sand incorporating induced lateral displacement to analyse the settlement and load-sharing behaviour, bending moment behaviour of raft and piles in PRF. Parametric study is carried out considering both uniform (UPL) and non-uniform pile length (NUPL) configurations in which pile spacing, pile number, and raft-soil stiffness ratio are varied. Results show that for all considered pile spacings, due to induced lateral displacement average settlement increases, whereas differential settlement decreases for both configurations. The NUPL configuration shows lesser differential settlement than UPL configuration. The proportion of vertical and lateral load carried by piles in NUPL configuration is lesser and more, respectively, compared to that of UPL configuration. The NUPL configuration yielded a greater percentage reduction of average settlement due to increase in pile number. With the variation in raft stiffness from flexible to rigid, negative differential settlement is observed for NUPL configuration. The lateral load carried by piles in NUPL configuration is higher than that of UPL configuration for flexible rafts. The bending moment in raft is observed to be significantly lower in the case of NUPL configuration than UPL configuration. The piles in NUPL configuration show lesser bending moment at the pile head than that of UPL configuration for a rigid raft.

Keywords: Large piled-raft, Settlement, Load-sharing behavior, Bending moment.

M. Rokonuzzaman et al. (eds.), *Proceedings of the 7th International Conference on Civil Engineering for Sustainable Development (ICCESD 2024)*, Atlantis Highlights in Engineering 34,
https://doi.org/10.2991/978-94-6463-478-5_9

1 Introduction

The piled-raft foundation (PRF) is a hybrid foundation composed of two structural components, i.e., the raft and piles, and this foundation has emerged as one of the most popular alternative foundation types for high-rise buildings, bridges, towers, industrial plants, and offshore constructions in modern construction techniques. According to the design concept of this foundation type, the entire superstructure load is transferred to the underlying soil by the combined resistance of both structural components. As a result, PRF achieves economy as compared to conventional pile foundations but exhibits a complex load-transfer mechanism. Large piled-rafts are those in which the width of the raft is larger compared to the length of the piles ($B_r/L > 1$), with the raft width greater than 15 m. This type of piled-raft generally has an adequate factor of safety, and hence, the bearing capacity of the foundation is not a major concern, but the average and differential settlements of the foundation become a significant problem. The outcomes of most of the past research work on piled-rafts have resulted in the establishment of design practices for piled-rafts either under pure vertical loading or pure lateral loading cases [1-4]. However, the piled-raft foundations for onshore structures practically are not only subjected to vertical loads but lateral displacement can also be induced in the piled-rafts due to various situations such as the excavations carried out very close to the existing PRF, earthquake shaking, etc. Further, the majority of earlier studies concentrated on offering design guidelines for piled-rafts with uniform pile lengths due to the ease of construction and to reduce the chance of error during pile installation. According to the statistics revealed by the Council of Tall Buildings and Urban Habitat (CTBUH) in the year 2018, there are 146 completed high-rise structures worldwide that are 200 m or taller founded on pile foundation or PRF with non-uniform pile length (NUPL) configurations [5]. Moreover, in recent years, the research work concerning the design of PRF considering NUPL also gained attention, but limited studies have been found for such type of configuration, incorporating an induced lateral displacement in addition to vertical loads.

Hence, the objective of the present study is to investigate the varying responses of vertically loaded large PRF in dense sand due to the incorporation of an induced lateral displacement by performing a parametric study considering both uniform pile length and non-uniform pile length configurations. The effects of piled-raft geometric parameters such as the pile spacing, pile number, and raft-soil stiffness ratio on the average settlement, differential settlement, vertical load-sharing ratio, lateral load-sharing ratio, raft bending moment and pile bending moment profile are analyzed.

2 Numerical Modeling

In this section, the systematic procedure of numerical modeling of large piled-raft foundations in sandy soil is described along with the validation studies. Three-dimensional numerical modeling is carried out with the help of Plaxis 3D software, which is based on the finite element method.

2.1 Domain Size and Meshing Details

The lateral extent of the soil domain is fixed at a distance of 4.5 times the raft width (B_r) from the raft edge on all four sides and the vertical depth of the soil domain is fixed at 7 times the pile length (L_p) from the base of the raft. The vertical boundaries of the soil domain on all four sides are assumed to be on rollers, meaning that vertical movements are only allowed and lateral movements are restrained. The bottom boundary is kept fixed; that is, both the vertical and lateral movements are restrained whereas the top ground surface is kept free in all directions. The boundaries of the soil model have been selected keeping in mind that the piled-raft influence zone is well within the soil domain to avoid any undesirable boundary effects. Fig. 1 shows the finite element model of the PRF with boundary conditions of the soil domain. Based on mesh convergence analysis, fine mesh is selected for modeling the soil domain and finer mesh is adopted near the structural elements where large deformations or stresses are concentrated.

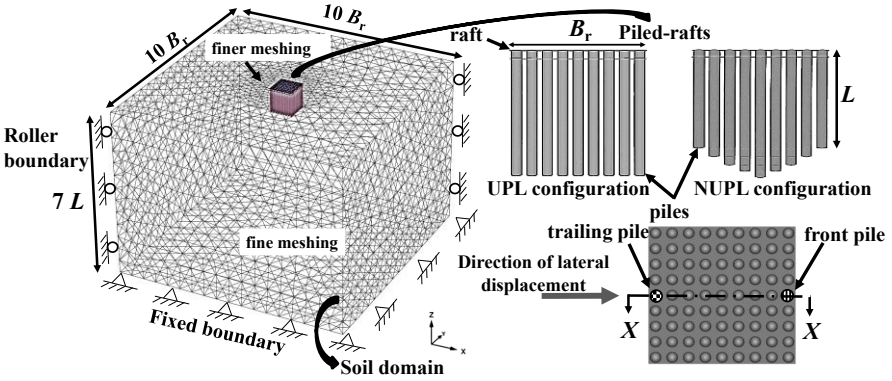

Fig. 1. Finite element model of piled-rafts with boundary conditions of soil domain

2.2 Simulation of Soil and Structural Elements

The soil volume consisting of soil elements is modeled with 10 node tetrahedral elements, whereas the structural elements, i.e., the raft and piles are modeled considering 6-node triangular plate elements and embedded beam elements, respectively. The interaction of the raft with the soil underneath it is modeled with 12 node interface elements, and a special interface element of the embedded beam is used to model the pile-soil interaction at the side and base of the pile. The reduced shear strength at the soil-structure interface is taken into account by the Interface Reduction Factor (R_{int}). In the present study, R_{int} value of 0.67 is considered because, for real soil-structure interaction, the interface is weaker and more flexible than the surrounding soil, and hence, the value of R_{int} is taken less than one (Plaxis 3D). The structural interaction between the raft and pile head is considered as a rigid connection. The non-linear stress-strain behavior of sandy soil is simulated using the Hardening Soil model,

which is based on the hyperbolic relationship between the deviatoric stress and axial strain. The behavior of both raft and pile are considered to be linear-elastic. The properties of the homogeneous dense sand, raft, and piles are shown in Table 1 [3].

Table 1. Input parameters for numerical model

Soil Properties	Dense Sand
Relative density (%)	70
Dry unit weight, γ_d (kN/m^3)	15.6
Secant Young's modulus , E_{50}^{ref} (MPa)	37.67
Oedometer stiffness, E_{oed}^{ref} (MPa)	37.67
Unloading/reloading stiffness, E_{ur}^{ref} (MPa)	115.2
Friction angle, ϕ (°)	43
Cohesion , c (kPa)	0
Poisson's ratio, υ	0.25
Stress dependency power	0.65
Dilatancy angle, ψ(°)	11
Raft and Pile Properties	
Modulus of elasticity, E (MPa)	30000
Poisson's ratio, υ	0.15
Unit weight, γ (kN/m^3)	25

2.3 Validation of Numerical Model

The ability of the presently developed 3D numerical model to provide reliable results is analyzed by performing a validation study with two experimental observations. The numerical model is validated with the centrifuge test results of Park and Lee [4] and Sawada and Takemura [6]. The first validation study is performed with reference to the vertical load vs. settlement results of Park and Lee [4] by modeling the soil domain and foundation on a prototype scale with an acceleration of 60 g. The piled-raft model with a square raft of size 9 m and 16 piles of diameter and length of 0.6 m and 15 m, respectively, are arranged in a 4 × 4 pile configuration with a pile spacing of 2.4 m. The linear elastic-perfectly plastic Mohr-Coulomb model is used for simulating the behavior of sandy soil. The elastic modulus (E) and the angle of internal friction (ϕ) of the dense sand having a relative density of 84% are taken as 50 MPa and 41°, respectively. The vertical load-settlement curves of the piled-raft foundation obtained from both numerical analysis and centrifuge test are presented in Fig. 2 (a). The centrifuge test result appears to predict a bit higher stiffness value; however, the overall response shows a reasonably close match with a similar trend of the numerical analysis.

The second validation study is carried out with reference to those of the centrifuge test results of Sawada and Takemura [6] to examine the lateral response of the piled-raft. The static vertical and horizontal loading tests are conducted on model piled-rafts embedded in Toyoura sand, under the centrifugal acceleration of 50 g. Initially, a pre-vertical load test is performed with a displacement-controlled loading intensity of

0.0162 mm/s. The total self-weight of the raft and superstructure are assumed to be 2.7 kg. Further, the push-in and push-out tests are performed by applying horizontal load at a height equivalent to the pile spacing (h/s = 1). For the present study, only the results concerning the first half of the push-in load test for h/s = 1 case are considered. Fig. 2 (b) presents the comparison of the horizontal load-displacement curve of the present study with those of the model test results, which indicates a good agreement.

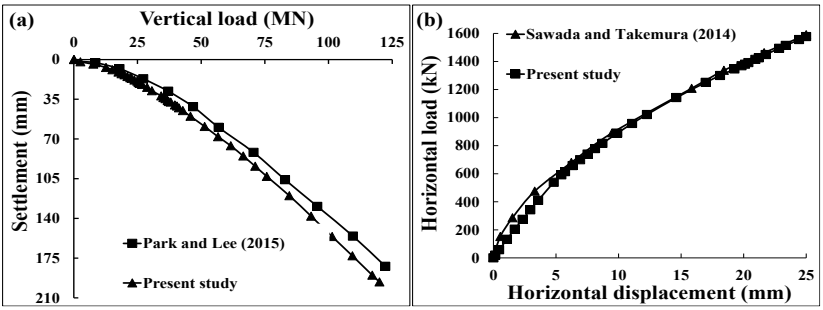

Fig. 2. Comparison of load vs settlement curve between computed and measured: (a) vertical loading and (b) combined vertical and lateral loading

2.4 Parametric Study

The responses of vertically loaded large PRF in dense sand due to the incorporation of an induced lateral displacement are investigated in this study. A parametric study is carried out considering a PRF with uniform pile length (UPL) and non-uniform pile length (NUPL) configurations under pure vertical loading (u_x = 0) and incorporation of an induced lateral displacement (u_x = 0.1 d), in which pile spacing (s), pile number (N_p), and raft-soil stiffness ratio (K_{rs}) are varied. The responses are plotted in the form of average settlement (W_{avg}), differential settlement (W_{diff}), vertical load-sharing ratio ($\alpha_{pr(v)}$), lateral load-sharing ratio ($\alpha_{pr(l)}$), raft bending moment (M_r) and pile bending moment (M_p) profile. A large PRF modeled in the finite element analyses is composed of a square raft of width (B_r) 25 m with varying raft thickness (t_r) and piles of varying geometric configurations. The t_r varying as 0.7 m, 1.4 m, 2 m, and 4.7 m corresponds to four different relative K_{rs} of 0.4 (flexible), 3 (intermediate flexible), 10 (rigid), and 117 (extremely rigid), respectively, calculated according to Horikoshi & Randolph (1998) given by Equation 1.

$$K_{rs} = 5.57 \frac{E_r}{E_s} \frac{1-\upsilon_s^2}{1-\upsilon_r^2} \left(\frac{B}{L}\right)^{\alpha} \left(\frac{t_r}{L}\right)^3 \quad (1)$$

Where E_r and E_s are Young's modulus of elasticity of the raft and soil at shallow depth, respectively; υ_r and υ_s are the Poisson's ratio of the raft and soil, respectively. B, L, and t_r are the width, length, and thickness of the raft, respectively. The s which is normalized with respect to pile diameter (d) is varied as s/d ratio of 2.5, 3, 4, 5 and 5.5 while N_p is varied as 9, 25, 49 and 81 keeping the B_g/B_r ratio of 0.92 (covering the

maximum raft area) fixed for all N_p. These varying parameters of the structural elements are shown in Table 2 along with all other standard raft and pile geometric parameters.

Table 2. Raft and pile geometric properties

Varying parameter	B_r (m)	K_{rs}	L (m)	D (m)	s (m)	N_p	B_g/B_r ratio
Effect of s/d ratio	25	0.4	25	1	2.5 d, 3 d, 4 d, 5 d, 5.5 d	25	0.4, 0.48, 0.64, 0.8, 0.88
Effect of N_p	25	0.4	25	1	11.5, 5.75, 3.83, 2.88	9, 25, 49, 81	0.92
Effect of K_{rs}	25	0.4, 3, 10, 114	25	1	5 d	25	0.8

The NUPL configuration is designed in such a way by keeping the pile length longer at the central region and gradually decreasing towards the raft edge, finally obtaining a V-shaped PRC. The layout of such a configuration adopts a squared variation pattern proposed by Leung et al. (2010) in which the piles of uniform length are arranged in a square pattern. The pattern function for the variation of the pile length is expressed by Equation 2.

$$\frac{l(i)}{r_0} = \frac{l_0}{r_0}\left[1 + \alpha i + \beta i\left(i - \frac{N-1}{2}\right)\right] \tag{2}$$

where l, l_0, r_0 are the pile length, length of the center pile, and pile radius, respectively; α and β represents the linear and curvature part in the variation of the pile length, respectively. N represents the number of rows and i is the index number, which indicates the grid number in which a particular pile is located counting from zero at the center pile. The piles in both UPL and NUPL configurations have the same total pile length indicating that the difference in PR response is due to the influence of the pile length variation and is regardless of the quantity of material that the piles consume. The applied vertical load considered in the study is 300 kPa, representing the equivalent vertical loading of a 30-storey building and the lateral displacement value of 10 % of the pile diameter (0.1 d) is applied to the piled-raft at the foundation level. The W_{avg} and W_{diff} are calculated by considering the settlement at the center (W_{center}) and at the corner (W_{corner}) of the raft and are calculated by Equation 3 (Reul & Randolph, 2004) and Equation 4, respectively, expressed as a percentage of B_r.

$$W_{avg} = \frac{1}{3}(2W_{center} + W_{corner}) \tag{3}$$

$$W_{diff} = (W_{center} - W_{corner}) \tag{4}$$

The permissible average and differential settlement criteria considered for the present study corresponds to a value of $W_{avg} \leq 100$ mm (0.4 % B_r) (Chanda et al. 2021) and $W_{diff} \leq 25$ mm (0.1 % B_r) (Reul & Randolph, 2004) respectively, and not allowing any raft negative W_{diff}. The vertical load shared between the raft and piles are measured by $\alpha_{pr(v)}$ which is defined as the ratio of vertical load carried by the piles to the total applied vertical load on the piled-raft. The vertical load carried by the piles is obtained by adding the axial loads measured at the individual pile heads. The lateral load shared between the raft and piles is expressed in terms of the $\alpha_{pr(l)}$, which is defined as the ratio of lateral load carried by the piles to the total lateral load carried by the piled-raft. The lateral load carried by the piles is estimated as the sum of the shear forces from the individual pile heads. The structural behavior of the raft is analyzed in terms of the bending moment, which is evaluated at the raft center portion, at section XX. The M_p is obtained for two different pile locations in the pile group i.e., front and trailing piles.

3 Results and Discussions

3.1 Effect of Pile Spacing

Settlement Behavior. Fig. 3(a) and 3(b) depict the effect of *s*/*d* ratio on W_{avg} and W_{diff} respectively, for UPL and NUPL configurations under $u_x = 0$ and $u_x = 0.1\ d$ loading conditions. From Fig. 3(a), for both UPL and NUPL configurations, the W_{avg} decreases due to an increase in *s*/*d* ratio from 2.5 to 5.5 for both loading conditions. For UPL configuration, the corresponding percentage reduction in W_{avg} is evaluated to be 31.1% and 24.5% for $u_x = 0$ and $u_x = 0.1\ d$, whereas for NUPL configuration, the corresponding percentage reduction in W_{avg} is evaluated to be 16.7% and 13.8% for $u_x = 0$ and $u_x = 0.1\ d$. From Fig. 3(b), for both UPL and NUPL configurations, a negative W_{diff} is observed for smaller *s*/*d* ratios (*s*/*d* ratio of 2.5, 3, and 4) for both $u_x = 0$ and $u_x = 0.1\ d$. For *s*/*d* ratio of 5, the positive W_{diff} of 0.01% B_r at $u_x = 0$ changes to negative W_{diff} of -0.04% B_r at $u_x = 0.1\ d$ for UPL configuration. However, for *s*/*d* ratio of 5.5, a positive W_{diff} of 0.04% B_r (UPL) and 0.02% B_r (NUPL) is observed for $u_x = 0.1\ d$ which is lower as compared to a positive W_{diff} of 0.09% B_r (UPL) and 0.06% B_r (NUPL) for $u_x = 0$. A lower W_{diff} is seen for NUPL as compared to UPL configuration for both loading conditions at *s*/*d* ratio of 5.5. This is due to the presence of longer length piles at the center in NUPL configuration, a higher resistance is offered at the raft center resulting in a lower differential settlement.

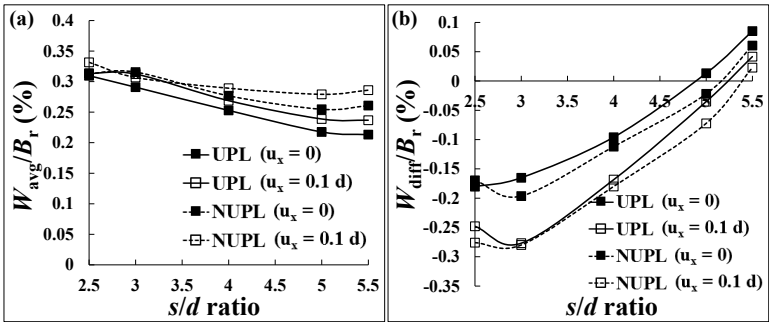

Fig. 3. Effect of *s*/*d* ratio on (a) average settlement and (b) differential settlement

Load-Sharing Behavior. Fig. 4(a) and 4(b) illustrate the effect of *s*/*d* ratio on $\alpha_{pr(v)}$ and $\alpha_{pr(l)}$ respectively, for UPL and NUPL configurations under $u_x = 0$ and $u_x = 0.1\ d$ loading conditions. From Fig.4(a), due to an increase in *s*/*d* ratio from 2.5 to 5.5, the vertical load carried by the piles in UPL increases by 77.8% and 72.6% for $u_x = 0$ and $u_x = 0.1\ d$ respectively, and piles in NUPL configuration increases by 56.8% and 60.8% for $u_x = 0$ and $u_x = 0.1\ d$ respectively. At larger pile spacing, the value of $\alpha_{pr(v)}$ in NUPL is lesser than UPL configuration because even though the raft causes confinement in both the configurations but to the shorter length of peripheral piles in NUPL, the mobilization of pile capacity is lesser as compared to the peripheral piles in UPL configuration. For both UPL and NUPL configurations, the $\alpha_{pr(v)}$ is observed to be higher for $u_x = 0.1\ d$ as compared to that of $u_x = 0$ for all *s*/*d* ratios. This is because in case of $u_x = 0.1$ d, the raft contact pressure decreases due to which the raft load share decreases and eventually leading to larger pile load share. From Fig.. 4(b), it is seen that due to an increase in *s*/*d* ratio from 2.5 to 5.5, the lateral load carried by the piles increases by 117.3% and 560% for UPL and NUPL configurations, respectively. No significant change in $\alpha_{pr(l)}$ is observed between the two configurations for larger *s*/*d* ratios.

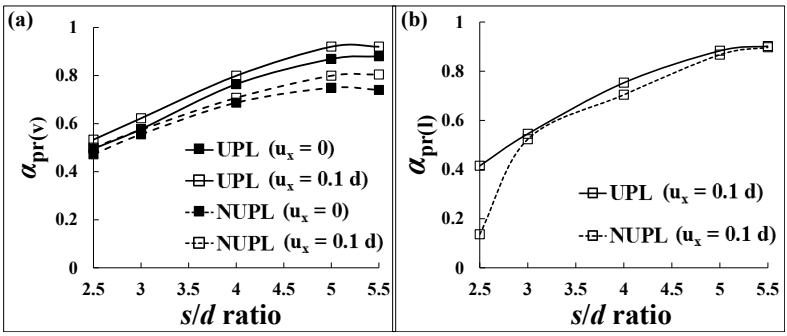

Fig. 4. Effect of *s*/*d* ratio on (a) vertical load-sharing ratio and (b) lateral load-sharing ratio

Bending Moment Behavior. Fig.5(a) and (b) portray the effect of s/d ratio on M_r along section XX for UPL and NUPL configurations respectively, under $u_x = 0$ and $u_x = 0.1\ d$. For both UPL and NUPL configurations, the M_r variation is observed to be higher for $u_x = 0.1\ d$ as compared to $u_x = 0$ for all s/d ratios. For both configurations, a negative M_r (observed at smaller s/d ratios) becomes negligible at larger s/d ratios for both loading conditions. There is no significant difference in M_r variation between UPL and NUPL configurations for all s/d ratios. Fig.6 and 7 illustrate the effect of s/d ratio on the M_p profile of the front and trailing piles in UPL and NUPL configurations respectively, under $u_x = 0$ and $u_x = 0.1\ d$.

From Fig.6 and 7, for both UPL and NUPL configurations, the increase in s/d ratio from 2.5 to 5.5 leads to a change in the M_p at the pile head from negative to positive (front pile) and positive to negative (trailing pile) for $u_x = 0$. However, for $u_x = 0.1\ d$, the increase in s/d ratio leads to an increase in the M_p at the pile head by 181.1% and 212% for UPL and NUPL, respectively (for front pile) and leads to a decrease in M_p by 42.3% and 37.8% for UPL and NUPL, respectively (for trailing pile). For both configurations, for $u_x = 0$, the M_p is observed as negative (front pile) and positive (trailing pile) at the pile head and becomes negligible from a depth of approx. 0.2 L for smaller s/d ratios (except s/d ratio of 5 to 5.5 where reverse happens). However, for $u_x = 0.1$ d, the M_p is positive at the pile head and showed a negative M_p from a depth of approx. (0.1-0.6) L for both front and trailing piles for all s/d ratios.

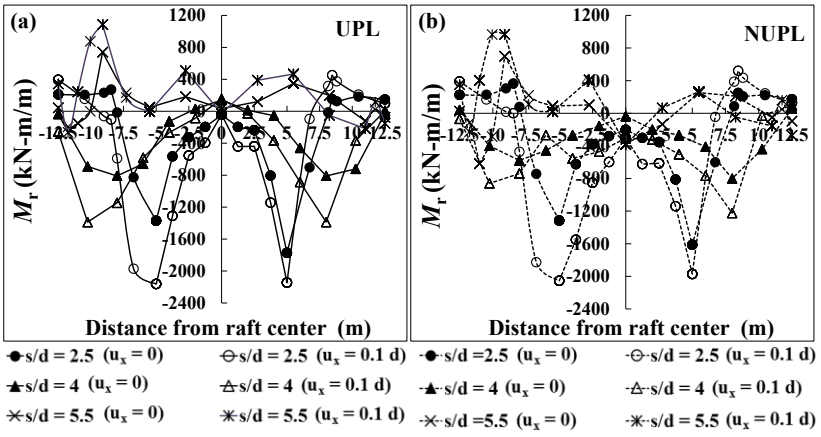

Fig. 5. Effect of s/d ratio on M_r behavior for (a) UPL and (b) NUPL configurations

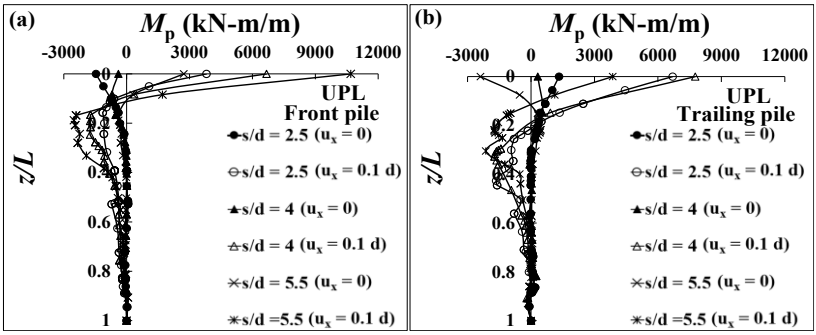

Fig. 6. M_p profiles of (a) front (b) trailing piles in UPL configuration for different *s*/*d* ratios

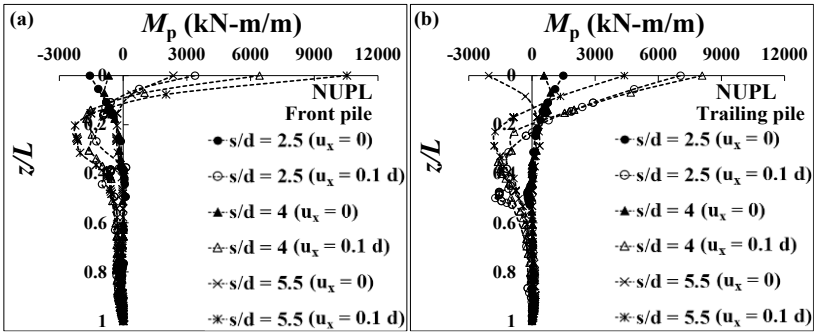

Fig. 7. M_p profiles of (a) front (b) trailing piles in NUPL configuration for different *s*/*d* ratios

3.2 Effect of Pile Number

Settlement Behavior. Fig. 8(a) and 8(b) show the effect of N_p on W_{avg} and W_{diff} respectively, for UPL and NUPL configurations under $u_x = 0$ and $u_x = 0.1\ d$. From Fig. 8(a), for both UPL and NUPL configurations, the W_{avg} decreases due to an increase in N_p under both loading conditions. For UPL configuration, due to an increase in N_p from 9 to 81, the corresponding percentage reduction in W_{avg} is evaluated to be 66.6% and 64.2% for $u_x = 0$ and $u_x = 0.1\ d$ respectively, whereas for NUPL configuration, the corresponding percentage reduction in W_{avg} is evaluated to be 47.7% and 44.6% for $u_x = 0$ and $u_x = 0.1\ d$, respectively. For all N_p, the W_{avg} is observed to be higher for $u_x = 0.1\ d$ as compared to that of $u_x = 0$, showing greater percentage increase at larger N_p as compared to smaller N_p for both configurations. From Fig. 8(b), W_{diff} decreases with increase in N_p for both configurations under both loading conditions; however, NUPL configuration at larger N_p under $u_x = 0.1\ d$ shows a negative W_{diff}. The W_{diff} is observed to be lower for $u_x = 0.1\ d$ as compared to that of $u_x = 0$ for all N_p. For $u_x = 0$, NUPL configuration exhibits lesser W_{diff} than UPL configuration for all N_p.

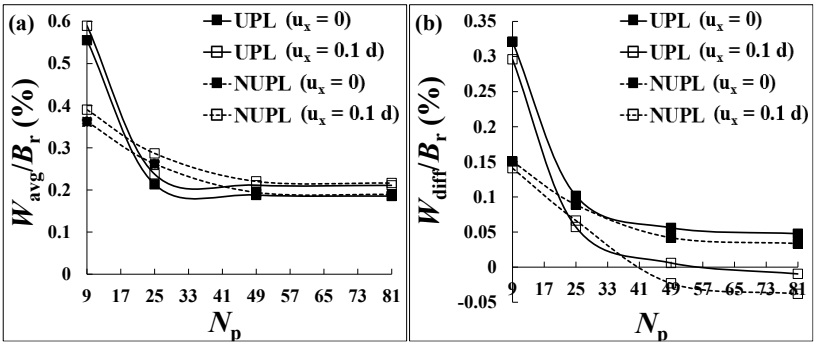

Fig. 8. Effect of N_p on (a) average settlement and (b) differential settlement

Load-Sharing Behavior. Fig. 9(a) and 9(b) illustrate the effect of N_p on $\alpha_{pr(v)}$ and $\alpha_{pr(l)}$ ratios respectively, for UPL and NUPL configurations under $u_x = 0$ and $u_x = 0.1\ d$. From Fig. 9(a), it is observed that with the increase in N_p from 9 to 49, the vertical load carried by the piles increases by 62.4% and 58.1% for $u_x = 0$ and $u_x = 0.1\ d$ respectively, for UPL configuration and increases by 193.9% and 173.6% for $u_x = 0$ and $u_x = 0.1\ d$ respectively, for NUPL configurations. Beyond $N_p = 49$, no significant increase in $\alpha_{pr(v)}$ is seen. For both UPL and NUPL configurations, there is no significant change in the $\alpha_{pr(v)}$ between $u_x = 0$ and $u_x = 0.1\ d$ for all N_p. From Fig. 9(b), for both UPL and NUPL configurations, $\alpha_{pr(l)}$ increases by 628% with an increase in N_p from 9 to 49. For all N_p, no significant change in $\alpha_{pr(l)}$ is observed between UPL and NUPL configurations

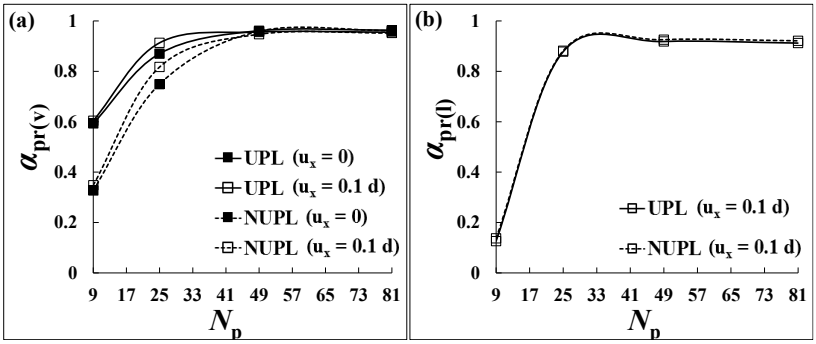

Fig. 9. Effect of N_p on (a) vertical load-sharing ratio and (b) lateral load-sharing ratio

Bending Moment Behavior. Fig. 10(a) and 10(b) illustrate the effect of N_p on M_r along section XX for UPL and NUPL configurations respectively, under $u_x = 0$ and $u_x = 0.1\ d$. For both loading conditions and configurations, the increase in the N_p from 9 to 25 significantly reduces the M_r; however, insignificant change is noticed for a further increase in N_p beyond 25. For both configurations, the M_r is slightly higher for $u_x = 0.1\ d$ as compared to $u_x = 0$ for all N_p. There is no significant difference in M_r varia-

tion between UPL and NUPL configurations for all N_p (except for N_p = 9, where NUPL configuration shows lower M_r variation).

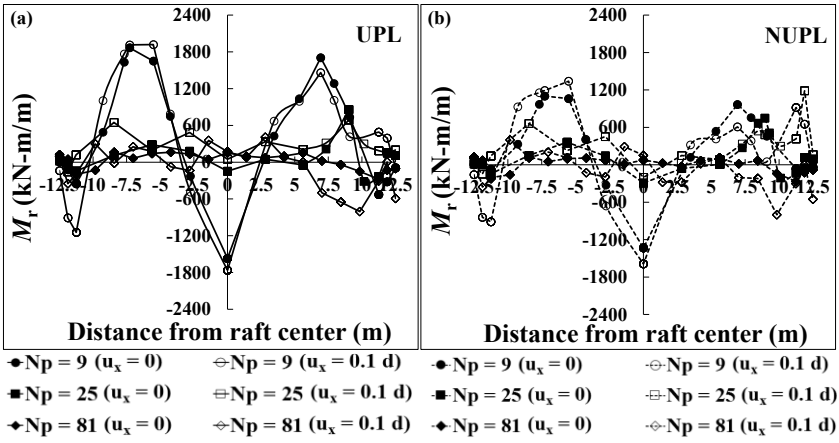

Fig. 10. Effect of N_p on M_r behavior for (a) UPL and (b) NUPL configurations

Fig. 11 and 12 illustrate the effect of N_p on the M_p profile of the front and trailing piles in UPL and NUPL configurations respectively, under u_x = 0 and u_x = 0.1 d. The increase in N_p from 9 to 25 leads to decrease in the M_p at the pile head by 81.1% and 68.3% for UPL and NUPL, respectively (for front pile) and decrease by 79.1% (negative M_p) and 68.4% (negative M_p) for UPL and NUPL, respectively (for trailing pile) for u_x = 0. Also, for u_x = 0.1 d, the increase in N_p leads to a decrease in the M_p at the pile head by 64.2% and 58.6% for UPL and NUPL, respectively (for front pile) and decrease by 33.9% and 56.8% for UPL and NUPL, respectively (for trailing pile). The front pile experiences larger M_p as compared to trailing pile for u_x = 0.1 d for both configurations.

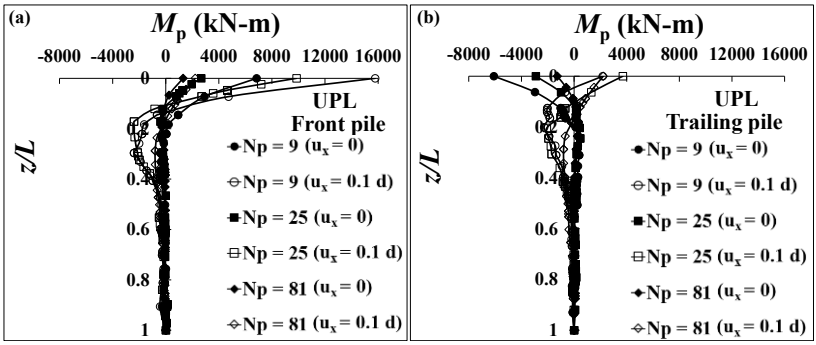

Fig. 11. M_p profiles of (a) front (b) trailing piles in UPL configuration for different N_p

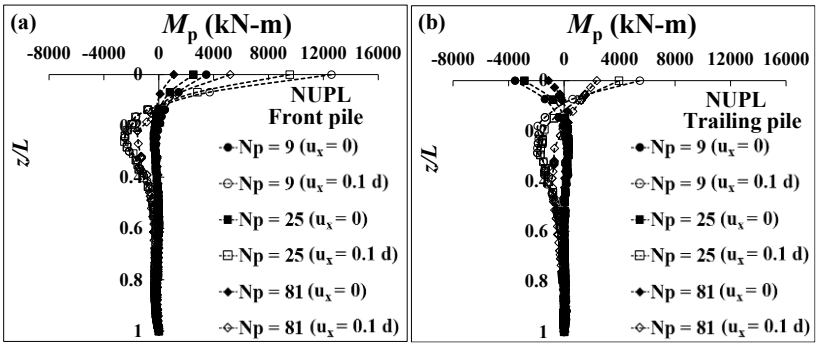

Fig. 12. M_p profiles of (a) front (b) trailing piles in NUPL configuration for different N_p

3.3 Effect of Relative Raft-Soil Stiffness Ratio

Settlement Behavior. Fig.13(a) and 13(b) show the effect of K_{rs} on W_{avg} and W_{diff}, respectively, for UPL and NUPL configurations under $u_x = 0$ and $u_x = 0.1\ d$. From Fig. 13(a), for both UPL and NUPL configurations, the W_{avg} increases due to an increase in K_{rs} under both $u_x = 0$ and $u_x = 0.1\ d$ conditions. For UPL configuration, due to an increase in K_{rs} from 0.4 to 114, the corresponding percentage increase in W_{avg} is evaluated to be 11.8% and 8.2% for $u_x = 0$ and $u_x = 0.1\ d$ respectively, whereas for NUPL configuration, the corresponding percentage increase in W_{avg} is evaluated to be 22.4% and 22.5% for $u_x = 0$ and $u_x = 0.1\ d$ respectively. For all K_{rs}, the W_{avg} is observed to be higher for $u_x = 0.1\ d$ as compared to that of $u_x = 0$ (for both configurations), showing a smaller percentage increase at higher K_{rs} value as compared to lower K_{rs} value for UPL configurations. From Fig. 13(b), the increase in K_{rs} value leads to a reduction in W_{diff} as expected (UPL configuration at $u_x = 0$). For $u_x = 0.1\ d$, the W_{diff} is observed to be negative for all K_{rs} values for both UPL and NUPL configurations. For $u_x = 0$, only the NUPL configuration with lower K_{rs} value ($K_{rs} = 0.4$ and 3) is seen to exhibit negative W_{diff}.

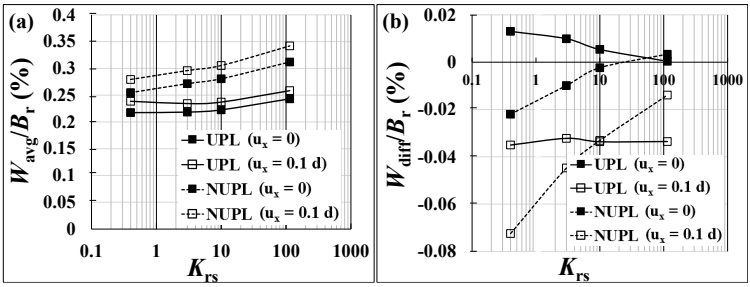

Fig. 13. Effect of K_{rs} on (a) average settlement and (b) differential settlement

Load Sharing Behavior. Fig. 14(a) and 14(b) show the effect of K_{rs} on $\alpha_{pr(v)}$ and $\alpha_{pr(l)}$ respectively, for UPL and NUPL configurations under $u_x = 0$ and $u_x = 0.1\ d$. For both configurations and loading conditions, the increase in K_{rs} values from 0.4 to 114 leads to a reduction in $\alpha_{pr(v)}$ and $\alpha_{pr(l)}$. From Fig. 14(a), the percentage reduction in $\alpha_{pr(v)}$ is evaluated as 16% and 14.6% for $u_x = 0$ and $u_x = 0.1$ d respectively, for UPL configuration while for NUPL configuration, the reduction is evaluated as 17.8% and 17.4% for $u_x = 0$ and $u_x = 0.1$ d, respectively. From Fig. 14(b), the percentage reduction in $\alpha_{pr(l)}$ is evaluated as 80% and 70.8% for UPL and NUPL configurations, respectively.

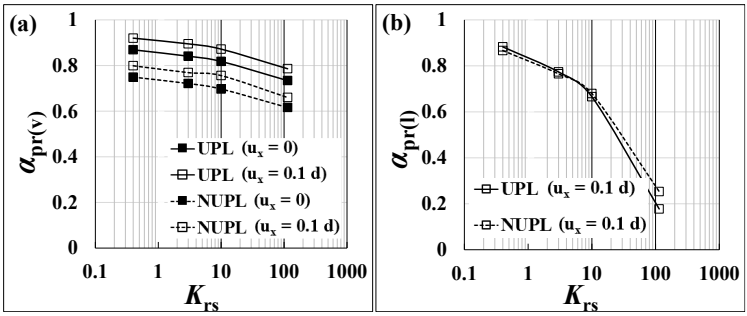

Fig. 14. Effect of K_{rs} on (a) vertical load-sharing ratio and (b) lateral load-sharing ratio

Bending Moment Behavior. Fig. 15(a) and 15(b) illustrate the effect of K_{rs} on M_r along section XX for UPL and NUPL configurations respectively, under $u_x = 0$ and $u_x = 0.1\ d$. For UPL configurations, for $u_x = 0$, the M_r is observed to be symmetric, with positive BM seen at the raft central region and the edges, which increases with an increase in K_{rs} value. However, for $u_x = 0.1\ d$, the M_r becomes asymmetric with a maximum positive M_r in the section observed towards the trailing row piles and a maximum negative M_r towards the side of front row piles. For NUPL configurations, for $u_x = 0$, the M_r at the raft central region becomes negative, which increases with an increase in K_{rs} value. For $u_x = 0.1\ d$, the maximum negative M_r is observed to be higher for NUPL as compared to UPL configuration.

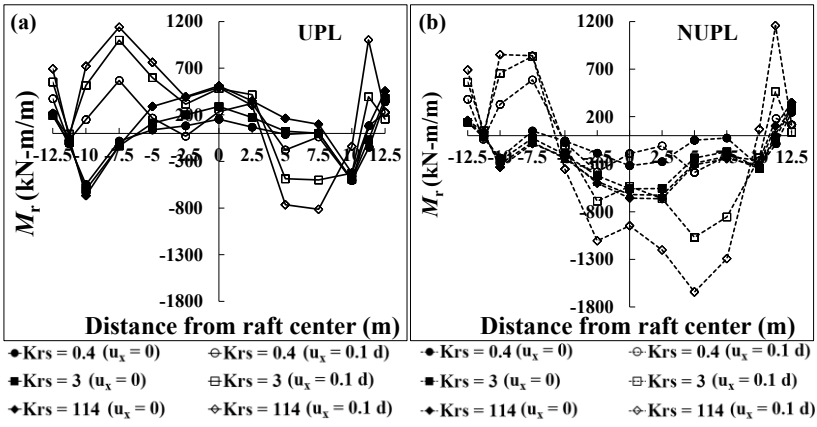

Fig. 15. Effect of K_{rs} on M_r behavior for (a) UPL and (b) NUPL configurations

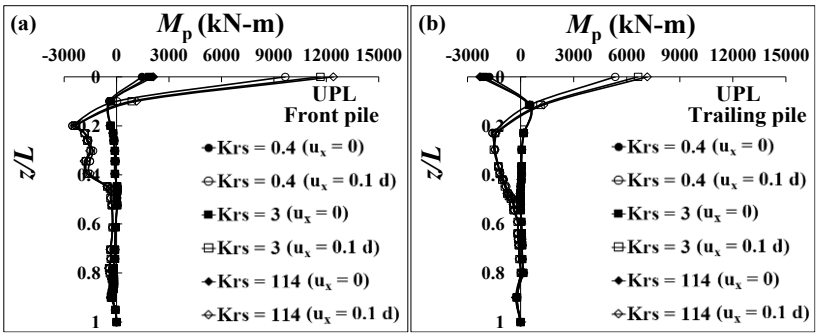

Fig. 16. M_p profiles of (a) front (b) trailing piles in UPL configuration for different K_{rs}

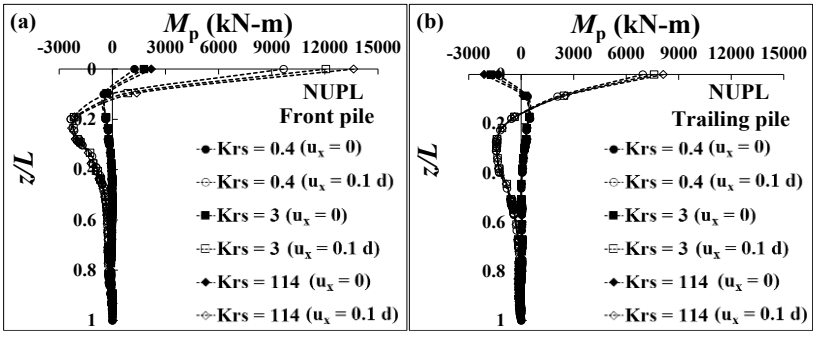

Fig. 17. M_p profiles of (a) front (b) trailing piles in NUPL configuration for different K_{rs}

Fig. 16 and 17 portray the effect of K_{rs} on the M_p profile of the front and trailing piles in UPL and NUPL configurations respectively, under $u_x = 0$ and $u_x = 0.1$ d. The increase in K_{rs} from 0.4 to 114 leads to increase in the M_p at the pile head by 44% and 75.6% for UPL and NUPL, respectively (for front pile) and increase by 29.8% (negative M_p) and 59.7% (negative M_p) for UPL and NUPL, respectively (for trailing pile) for $u_x = 0$. Also, for $u_x = 0.1$ d, the increase in K_{rs} leads to an increase in the M_p at the pile head by 28.6% and 40.8% for UPL and NUPL, respectively (for front pile) and increase by 33.9% and 17% for UPL and NUPL, respectively (for trailing pile).

4 Conclusions

From the numerical modeling results obtained, the following conclusions can be drawn:

1. The NUPL configuration is not effective in reducing average settlement as compared to UPL configuration for both loading conditions. The NUPL configuration exhibits lower differential settlement as compared to UPL configuration for both loading conditions for larger pile spacing. The vertical load-sharing ratio is lesser for NUPL in comparison to UPL for both loading conditions. The lateral load-sharing ratio depends on pile spacing but is independent of type of configuration at larger pile spacing. For both configurations and loading conditions, larger pile spacing helps to eliminate raft negative bending moment.
2. The NUPL configuration with smaller pile number exhibits lower raft bending moment as compared to UPL configuration for both loading conditions. For both configurations, lateral load-sharing ratio increases significantly due to an increase in pile number. The front pile experiences larger bending moment as compared to trailing pile for $u_x = 0.1\ d$ for both configurations for all pile numbers.
3. For all raft-soil stiffness ratio, NUPL configuration gives larger average settlement as compared to UPL for both loading conditions. The percentage reduction in both vertical load-sharing ratio due to increase in raft-soil stiffness ratio is lower for $u_x = 0.1\ d$ as compared to $u_x = 0$ for both configurations. The lateral load-sharing ratio decreases significantly with increasing raft-soil stiffness ratio for both configurations. For all raft-soil stiffness ratio, the value of maximum negative raft bending moments in NUPL is larger than UPL for $u_x = 0.1\ d$.

Acknowledgments
The authors acknowledge the Department of Civil Engineering, IIT Guwahati, for providing the necessary computing facilities.

References

1. Horikoshi K, Randolph M F. (1998) A contribution to optimum design of piled rafts. *Geotechnique*, 48(3): 301-317.
2. Reul O, Randolph M F. (2004) Design strategies for piled rafts subjected to nonuniform vertical loading. *Journal of Geotechnical and Geoenvironmental Engineering*, 130(1): 1-13.
3. Nguyen D D C, Jo S B, Kim D S. (2013) Design method of piled-raft foundations under vertical load considering interaction effects. *Computers and Geotechnics*, 47: 16-27.
4. Park D, Lee J. (2015) Comparative analysis of various interaction effects for piled rafts in sands using centrifuge tests. *Journal of Geotechnical and Geoenvironmental Engineering*, 141(1): 04014082.
5. Chanda D, Saha R, Haldar S. (2022) Influence of combined loading on static response of optimum CPRF with non-uniform pile length configurations. *Innovative Infrastructure Solutions*, 7(2): 170.
6. Sawada K, Takemura J. (2014) Centrifuge model tests on piled raft foundation in sand subjected to lateral and moment loads. *Soils and Foundations*, 54(2): 126-140.
7. Leung Y F, Klar A, Soga K. (2010) Theoretical study on pile length optimization of pile groups and piled rafts. *Journal of geotechnical and geoenvironmental engineering*, 136(2): 319-330.